CrossMark

Enhanced thermoelectric performance in *p*-type polycrystalline SnSe by Cu doping

Jiaran Li[1,2] · Jingtao Xu[1] · Hongxiang Wang[1] · Guo-Qiang Liu[1] · Xiaojian Tan[1] · Hezhu Shao[1] · Haoyang Hu[1] · Jun Jiang[1]

Abstract

Polycrystalline $Sn_{1-x}Cu_xSe$ samples have been prepared using hot pressing to study the Cu doping effect on carrier concentration in SnSe. Different from Ag, Cu doping decreases the carrier concentration of SnSe at room temperature. The carrier concentration of Cu doped samples increases obviously with temperature, becomes larger than the pristine sample above 523 K, and approaches the values of Na doped SnSe at 773 K. The enhanced carrier concentration leads to better electrical conductivity, resulting in higher power factors at high temperatures. Due to carrier optimization by Cu, a peak *ZT* of 0.66 is achieved in $Sn_{0.98}Cu_{0.02}Se$ at 813 K.

1 Introduction

With the increasing tension in energy resources and demand of economic growth in the world, renewable energy sources are becoming more and more important in recent years. Thermoelectric materials can be used for the direct conversion of heat to electricity and thus have attracted great attention for power generation [1–3]. The conversion efficiency of thermoelectric materials is determined by the dimensionless figure of merit, $ZT = S^2\sigma T/\kappa$, where S, σ, T, and κ are the Seebeck coefficient, electrical conductivity, absolute temperature, and thermal conductivity, respectively [4]. In order to achieve a high thermoelectric performance, power factor ($S^2\sigma$) should be enlarged, and meanwhile thermal conductivity, especially lattice thermal conductivity, must be minimized [5]. As both S and $S^2\sigma$ are related to the carrier concentration [6], the carrier optimization is one of the most useful way to enhance the thermoelectric performance.

Recent studies show that tin selenide (SnSe) processes very low thermal conductivity with a low carrier concentration ($\sim 10^{17}/cm^3$ at room temperature) in its single crystals [7]. Increasing carrier concentration is very efficient to improve thermoelectric performance of this material. A *ZT* of 2 at 800 K has been achieved in Na doped SnSe single crystal [8]. Many efforts have been paid to tune the carrier concentration of SnSe, and both *n*-type and *p*-type SnSe have been reported [9–31]. Alkali elements (Li, Na, K) [24–30] have been proven to be effective dopants in *p*-type polycrystalline SnSe. Among them, Na has been found to be the most effective one. On the other hand, Ag has also reported to be an effective dopant [10, 11, 31], Cu, the same group with Ag, has recently been used to tune carrier concentration of SnSe [32–34].

In this work, we synthesized polycrystalline Cu-doped SnSe by traditional melting and hot pressing. Different from previous reports, our Hall experiments show the carrier concentration decreases after Cu doping. However, the electrical conductivity does enhance at high temperatures, leading to larger *ZT* values in Cu doped samples. A peak *ZT* of 0.66 was obtained at 813 K for $Sn_{0.98}Cu_{0.02}Se$ perpendicular to the pressing direction.

2 Experimental section

2.1 Synthesis

Commercial elemental Sn granules (99.999%), Se granules (99.999%), and Cu powder (99.9%) were weighed according

✉ Jingtao Xu
   xujingtao@nimte.ac.cn

✉ Jun Jiang
   jjun@nimte.ac.cn

1   Ningbo Institute of Materials Technology and Engineering, Chinese Academy of Science, Ningbo 315201, China

2   Nano Science and Technology Institute, University of Science and Technology of China, Suzhou 215123, China

to the stoichiometry of $Sn_{1−x}Cu_xSe$ ($x = 0$, 0.01, 0.02, 0.03), and the mixtures were loaded into quartz tubes. For a typical experiment the following amounts were used: Sn (10.8368 g, 91.30 mmol), Se (7.4317 g, 94.12 mmol), and Cu (0.1794 g, 2.82 mmol) were used to prepare 15 g of $Sn_{0.97}Cu_{0.03}Se$. The tubes were evacuated to $\sim 3.2 \times 10^{−1}$ Pa and sealed. The quartz tubes were heated up to 1193 K in a rocking furnace, kept at this temperature for 1 h, and then air-quenched. The ingots were crashed into powder using ball milling in SPEX 8000M Mixer/Mill for 15 min. The powders were subsequently densified by hot pressing at 753 K for 10 min under a pressure of 60 MPa, producing columnar samples of ~ 13 mm in diameter and ~ 10 mm in height. The density (ρ) was measured using the Archimedes method, and the density of all samples is larger than 98% of the theoretical density, as shown in Table 1.

2.2 Characterization

The phase structure of all samples was examined by X-ray diffraction (XRD, Bruker D8, Germany) using the Cu Kα radiation ($\lambda = 1.5406$ Å) at room temperature. The surface of the samples was observed using scanning electron microscopy (SEM, Quanta FEG 250, FEI, USA). Energy-dispersive X-ray Spectrometry (EDS) was perform using the detector attached to SEM. The Seebeck coefficient and electrical conductivity of samples were measured by a Seebeck coefficient/electrical resistance measuring system (ZEM-3, Ulvac-Riko, Japan) under helium atmosphere from 300 to 813 K. The room temperature Hall coefficients (R_H) were measured using a Quantum Design Physical Properties Measurement System (PPMS-9) in magnetic fields ranging from $−5 \sim 5$ T. Hall carrier concentration (n_H) and mobility (μ_H) were calculated via $n_H = 1/(eR_H)$ and $\mu_H = \sigma R_H$, respectively. The Hall coefficients at high temperatures are measured using a home-made apparatus. Thermal diffusivity (D) was measured by a laser flash method (LFA457, Netzsch, Germany). The specific heat capacity (C_P) was taken from previous reports [7]. The thermal conductivity was calculated from $\kappa = DC_P\rho$.

3 Results and discussion

XRD patterns of both undoped and doped SnSe polycrystalline samples are shown in Fig. 1. All the peaks can be indexed to the orthorhombic phase with a *Pnma* symmetry. Structural anisotropy is clearly observed from the obvious difference in the relative peak intensity of (111) and (400), when measured in different directions as shown in Fig. 1a, b. But the ratio of peak intensity between (400) and (111) is much smaller than those in previous reports [11, 13], suggesting that the anisotropy is reduced probably because of the ball-milling process.

Figure 2 shows the SEM results for the $Sn_{0.98}Cu_{0.02}Se$ sample. In Fig. 2a, the fractured surface of $Sn_{0.98}Cu_{0.02}Se$ is shown. Grains with size smaller than 1 μm can be clearly seen in Fig. 2a. Due to the high energy ball-milling, the grain size is significantly reduced. Such a result is consistent with

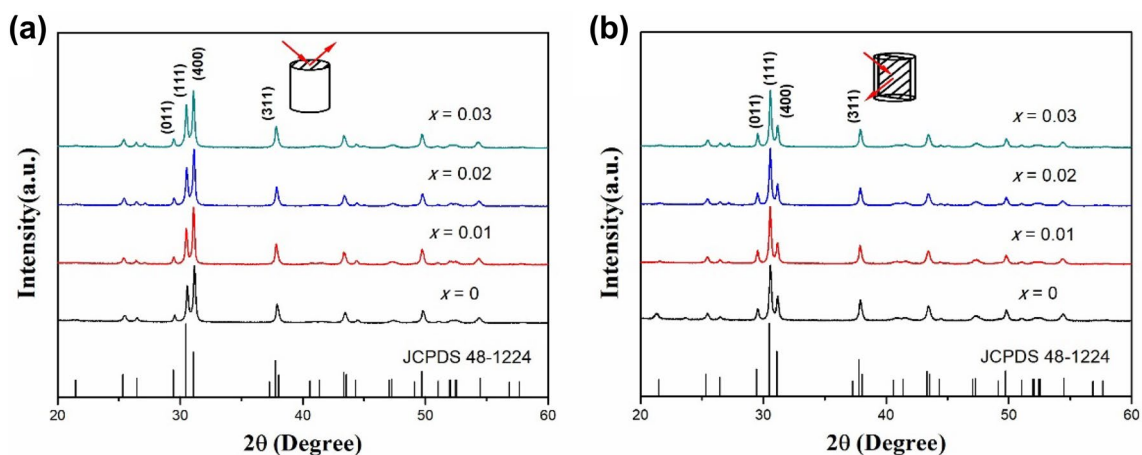**Table 1** The density, room temperature carrier concentration, mobility, Seebeck coefficient and high temperature carrier concentration of $Sn_{1−x}Cu_xSe$ ($x = 0$, 0.01, 0.02, 0.03) samples in the direction perpendicular to pressure

x	Density (g/cm³)	n_{H_RT} (10^{15}/ cm³)	μ (cm²/V s)	S (μV/K)	n_{H_773K} (10^{19}/ cm³)
0	6.11	262	0.61	635	–
0.01	6.17	4.53	6.01	680	1.44
0.02	6.16	3.54	4.24	684	1.54
0.03	6.17	3.94	3.89	639	1.69

Fig. 1 XRD patterns of $Sn_{1−x}Cu_xSe$ ($x = 0$, 0.01, 0.02, 0.03) polycrystalline samples perpendicular (**a**) and parallel (**b**) to the pressing direction
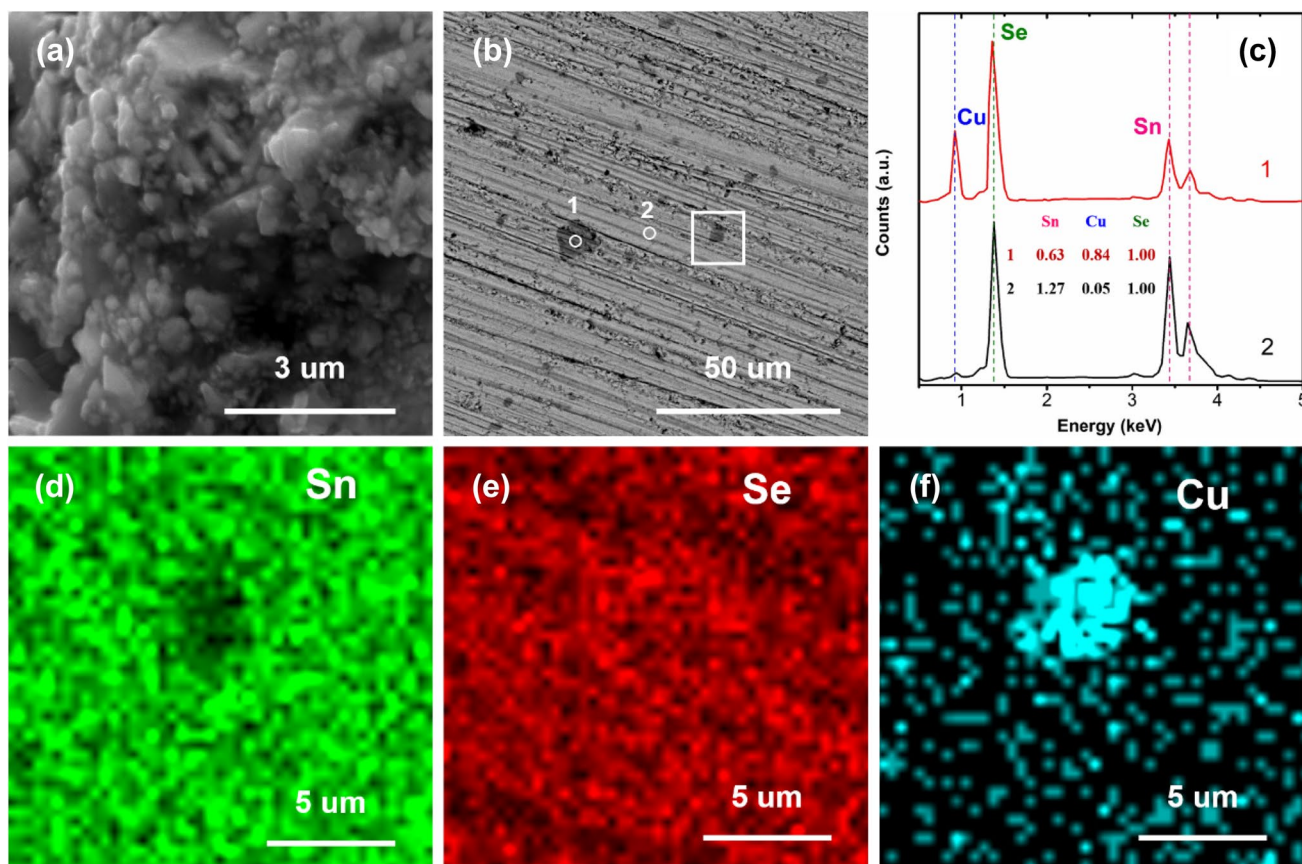
Fig. 2 **a** Fractured and **b** polished surface morphologies of the $Sn_{0.98}Cu_{0.02}Se$ sample. **c** The corresponding EDS results for spot 1 and 2 in (**b**). EDS mapping result of the selected region in (**b**): **d** Sn, **e** Se, and **f** Cu, respectively

the one from XRD. In Fig. 2b, the polished surface of the same sample is shown. Some obvious second phases can be observed from the picture. Elemental maps of Sn, Se and Cu from the selected region indicated in Fig. 2b, show elemental inhomogeneity of the specimen, as shown in Fig. 2d–f. The mapping results show that the second phase is rich in copper and lacks Sn. The point EDS analysis further confirms that the second phase is close to $Cu_4Sn_3Se_5$, as shown in Fig. 2c. The presence of the second phase suggests a low solid solution limit of copper in the SnSe lattice. The thermoelectric properties as a function of temperature for $Sn_{1-x}Cu_xSe$ ($x = 0$, 0.01, 0.02, 0.03) samples are shown in Fig. 3. In Fig. 3a, the temperature dependence electrical conductivity (σ) measured perpendicular to the pressing direction are plotted. The conductivity of both undoped and doped SnSe increase with temperature in the whole temperature range, and the increase becomes obvious above 673 K. The increase of electrical conductivity from 673 to 813 K could be attributed to the thermal activation of minority carriers due to the temperature dependent reduction of the band gap from the well-known *Pnma-Cmcm* phase transition [3, 35]. With increasing Cu content, the obvious enhancement of

electrical conductivity at high temperatures is observed, suggesting additional hole injections from Cu. The highest electrical conductivity is 53 S/cm at 813 K for $Sn_{1.97}Cu_{0.03}Se$. But when we analyze the room temperature data, the electrical conductivity decreases with increasing Cu, as shown in Table 1. The room temperature Hall measurement confirms that the carrier concentration reduces after introduction Cu (Table 1). Such results are completely different from our assumption and the data at high temperatures.

To further understand the electrical properties of Cu doped SnSe, high-temperature Hall measurements were carried out in Chongqing University. The results are shown in Fig. 4. It can be seen that the carrier concentration dropped by two orders of magnitude at room temperature on account of the introduction of Cu, consistent with our room temperature measurement. And the carrier concentration of Cu-doped SnSe increases with increasing temperature in the whole temperature range. A crossover at 523 K is observed. Above this temperature, Cu doped SnSe samples show higher carrier concentration than the undoped one. A hump at 600 K is found in $x = 0.01$ and 0.02, which needs further confirmation. With the further
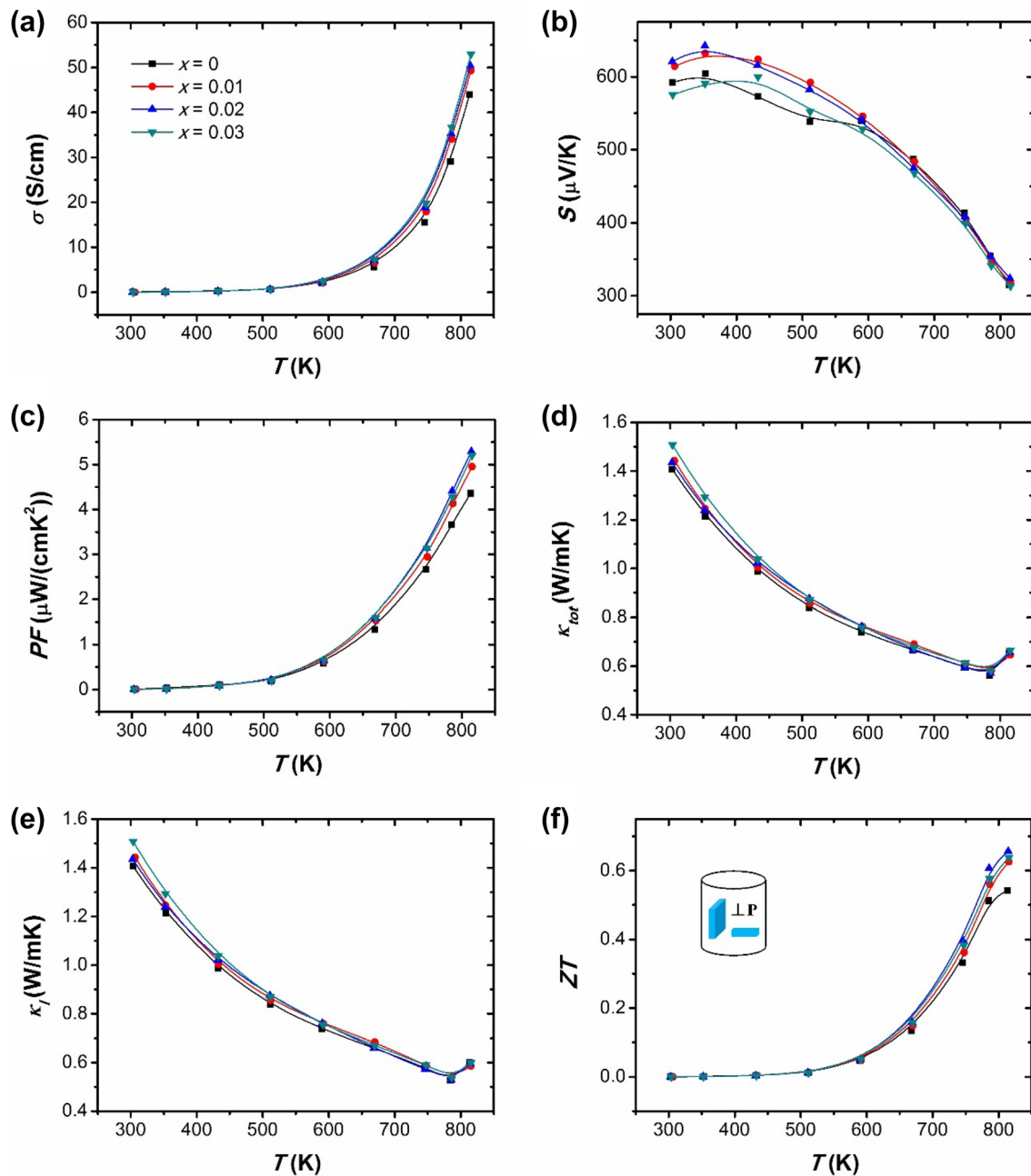
Fig. 3 Temperature dependence of **a** electrical conductivity, **b** Seebeck coefficient, **c** power factor, **d** total thermal conductivity, **e** lattice thermal conductivity, and **f** ZT for $Sn_{1-x}Cu_xSe$ ($x=0$, 0.01, 0.02, 0.03) polycrystalline samples measured perpendicular to the pressing direction

increase of temperature, the carrier concentration of Cu-doped SnSe reaches the value for 1% Na-doped SnSe at 773 K, suggesting that Cu is an effective p-type dopant for SnSe at high temperatures. Here, the reason for the continuous increase in the carrier concentration of Cu-doped SnSe still needs to be clarified. One possible reason may be the thermal activation of minority carriers, and the crossover may originate from the complicated phase diagram of Cu_2Se–SnSe.

Figure 3b shows the Seebeck coefficient of $Sn_{1-x}Cu_xSe$ ($x=0$, 0.01, 0.02, 0.03) samples perpendicular to the pressing direction. All samples show similar temperature dependence. Due to the subdued carrier concentration, Cu doped samples roughly show higher Seebeck coefficients than the undoped one at low temperatures. The largest Seebeck coefficient is about 640 μV/K at 350 K for $Sn_{0.98}Cu_{0.02}Se$. The Seebeck coefficient of all samples decreases as the temperature increases. Considering the fact that the carrier
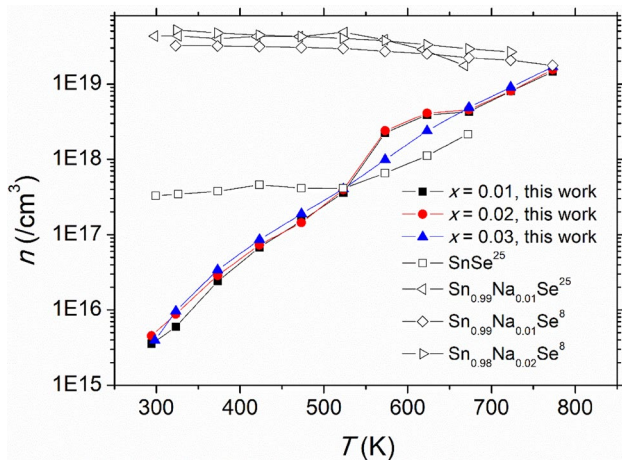
Fig. 4 Hall carrier concentration varying with temperature for polycrystalline samples of SnSe

concentration also increases, the behaviors could be attributed to the thermal activation of minority carriers across the band gap [7]. The power factors as a function of temperature for $Sn_{1-x}Cu_xSe$ ($x = 0, 0.01, 0.02, 0.03$) samples are shown in Fig. 3c. Due to enhancement of electrical conductivity at high temperatures after Cu doping, the improvement in power factors can be observed. A maximum power factor of about 5.3 $\mu W\ cm^{-1}\ K^{-1}$ has been obtained at 813 K for $Sn_{0.98}Cu_{0.02}Se$, which is larger than the value for reported Cu-doped SnSe [32, 33]. Such results demonstrated that the introduction of Cu actually contributes to the enhancement of electrical performance of SnSe polycrystalline.

The temperature dependence of the total thermal conductivity (κ) of the $Sn_{1-x}Cu_xSe$ ($x = 0, 0.01, 0.02, 0.03$) samples is shown in Fig. 3d. We can see that the thermal conductivity decreases with increasing temperature until about 800 K. And then a transition is observed, which should be the structural transition from *Pnma* to *Cmcm*. Above the transition, the thermal conductivity sharply rises at higher temperatures. The lowest thermal conductivity is found at the transition temperature, 0.56 W/m·K at 785 K for doped SnSe. The decrease is attributed to the dominant phonon–phonon interaction and the rise is probably attributed to the bipolar excitation [35]. The lattice thermal conductivity (κ_L) calculated by subtracting the electronic part from the total thermal conductivity using $\kappa_e = L\sigma T$, where L is the Lorenz number. The calculated κ_L was shown in Fig. 3e. The overall behavior of κ_l is very similar to total thermal conductivity, since the phonon transport dominates the thermal conductivity in SnSe. The lowest lattice thermal conductivity is 0.52 W/m·K at 785 K for undoped SnSe.

Figure 3f shows the temperature dependence of TE figure of merit ZT for $Sn_{1-x}Cu_xSe$ samples. The undoped SnSe matrix displays a maximum ZT around 0.54 at 813 K. Due to the introduction of Cu, the maximum ZT is improved to 0.66 at 813 K. This suggests that Cu is an effective p-type dopant in improving the thermoelectric performance of polycrystalline SnSe at high temperatures.

4 Conclusion

Cu-doped SnSe bulk samples have been prepared using ball milling and hot pressing. Cu doping decreases the carrier concentration at room temperature, but enhance the carrier concentration above 523 K, suggesting that Cu is an effective p-type dopant at high temperatures. After Cu doping, the electrical conductivity and power factor at high temperatures increase, which leads to a peck ZT of 0.66 at 813 K for $Sn_{0.98}Cu_{0.02}Se$ perpendicular to the pressing direction.

References

1. L.E. Bell, Science **321**, 1457 (2008)
2. G.J. Snyder, E.S. Toberer, Nat. Mater. **7**, 105 (2008)
3. D.M. Rowe, *Handbook of Thermoelectric* (CRC Press, Boca Raton, 1995)
4. M.G. Kanatzidis, Chem. Mater. **22**, 648 (2010)
5. Y.M. Han, J. Zhao, M. Zhou, X.X. Jiang, H.Q. Leng, L.F. Li, J. Mater. Chem. A **3**, 4555 (2015)
6. G.J. Tan, L.D. Zhao, F.Y. Shi, J.W. Doak, S.H. Lo, H. Sun, C. Wolverton, V.P. Dravid, C. Uher, M.G. Kanatzidis, J. Am. Chem. Soc. **136**, 7006–7017 (2014)
7. L.D. Zhao, S.H. Lo, Y.S. Zhang, H. Sun, G.J. Tan, C. Uher, C. Wolverton, V.P. Dravid, M.G. Kanatzidis, Nature **508**, 373 (2014)
8. K.L. Peng, X. Lu, H. Zhan, S. Hui, X.D. Tang, G.W. Wang, J.Y. Dai, C. Uher, G.Y. Wang, X.Y. Zhou, Energy Environ. Sci. **9**, 454 (2016)
9. D. Wu, L.J. Wu, D.S. He, L.D. Zhao, W. Li, M.H. Wu, M. Jin, J.T. Xu, J. Jiang, L. Huang, Y.M. Zhu, M.G. Kanatzidis, J.Q. He, Nano Energy **35**, 321–330 (2017)
10. M. Jin, H.Z. Shao, H.Y. Hu, D.B. Li, J.T. Xu, G.Q. Liu, H. Shen, J.Y. Xu, H.C. Jiang, J. Jiang, J. Cryst. Growth **460**, 112–116 (2017)
11. X. Wang, J.T. Xu, G.Q. Liu, X.J. Tan, D.B. Li, H.Z. Shao, T.Y. Tan, J. Jiang, NPG Asia Mater. **9**, e426 (2017)
12. D.B. Li, X.J. Tan, J.T. Xu, G.Q. Liu, M. Jin, H.Z. Shao, H.J. Huang, J.F. Zhang, J. Jiang, RSC Adv. **7**, 17906–17912 (2017)
13. Y.J. Fu, J.T. Xu, G.Q. Liu, J.K. Yang, X.J. Tan, Z. Liu, H.M. Qin, H.Z. Shao, H.C. Jiang, B. Liang, J. Jiang, J. Mater. Chem. C **4**, 1201 (2016)
14. P.C. Wei, S. Bhattacharya, J. He, S. Neeleshwar, R. Podila, Y.Y. Chen, A.M. Rao, Nature **539**, E1 (2016)
15. Z.H. Ge, D.S. Song, X.Y. Chong, F.S. Zheng, L. Jin, X. Qian, L. Zheng, R.E. Dunin-Borkowski, P. Qin, J. Feng, L.D. Zhao, J. Am. Chem. Soc. **139**, 9714–9720 (2017)

16. G.D. Tang, W. Wei, J. Zhang, Y.S. Li, X. Wang, G.Z. Xu, C. Chang, Z.H. Wang, Y.W. Du, L.D. Zhao, J. Am. Chem. Soc. **138**, 13647–13654 (2016)
17. Y.X. Chen, Z.H. Ge, M.J. Yin, D. Feng, X.Q. Huang, W.Y. Zhao, J.Q. He, Adv. Funct. Mater. **26**, 6836–6845 (2016)
18. J.C. Li, D. Li, X.Y. Qin, J. Zhang, Scr. Mater. **126**, 6–10 (2017)
19. Q. Zhang, E.K. Chere, J. Sun, F. Cao, K. Dahal, S. Chen, G. Chen, Z.F. Ren, Adv. Energy Mater. **5**, 1500360 (2015)
20. X. Wang, J.T. Xu, G.Q. Liu, Y.J. Fu, Z. Liu, X.J. Tan, H.Z. Shao, H.C. Jiang, T.Y. Tan, J. Jiang, Appl. Phys. Lett. **108**, 083902 (2016)
21. K.L. Peng, B. Zhang, H. Wu, X.L. Cao, A. Li, D.F. Yang, X. Lu, G.Y. Wang, X.D. Han, C. Uher, X.Y. Zhou, Mater. Today (2017)
22. Q. Zhang, E.K. Chere, J.Y. Sun, F. Cao, K. Dahal, S. Chen, G. Chen, Z.F. Ren, Adv. Energy Mater. **5**, 12 (2015)
23. L.J. Zhang, J.L. Wang, Q. Sun, P. Qin, Z.X. Cheng, Z.H. Ge, Z. Li, S.X. Dou, Adv. Energy Mater. **7**, 1700573 (2017)
24. E.K. Chere, Q. Zhang, K. Dahal, F. Cao, J. Mao, Z. Ren, J. Mater. Chem. A **4**, 1848 (2016)
25. T.R. Wei, G.J. Tan, X.M. Zhang, C.F. Wu, J.F. Li, V.P. David, G.J. Snyder, M.G. Kanatzidis, J. Am. Chem. Soc. **138**, 8875 (2016)
26. Z.R. Yang, W.H. Chen, C.J. Liu, J. Elect. Mater. **46**, 2964 (2017)
27. T.R. Wei, C.F. Wu, X. Zhang, Q. Tan, L. Sun, Y. Pan, J.F. Li, Phys. Chem. Chem. Phys. **17**, 30102 (2015)
28. H.Q. Leng, M. Zhou, J. Zhao, Y. Han, L.J. Li, Electron. Mater. **45**, 527 (2016)
29. B.W. Cai, J.H. Li, H. Sun, P. Zhao, F.R. Yu, L. Zhang, D.L. Yu, Y.J. Tian, B. Xu, J. Alloys Compd. **08**, 223 (2017)
30. H.Q. Leng, M. Zhou, J. Zhao, Y.M. Han, L.F. Li, RSC Adv. **6**, 9112 (2016)
31. C.L. Chen, H. Wang, Y.Y. Chen, T. Day, G.J. Snyder, J. Mater. Chem. A **2**, 11171 (2014)
32. N.K. Singh, S. Bathula, B. Gahtori, K. Tyagi, D. Haranath, A. Dhar, J. Alloys Compd. **668**, 152–158 (2016)
33. J. Gao, G.Y. Xu, Intermetallics **89**, 40–45 (2017)
34. X. Shi, K. Zheng, M. Hong, W. Liu, R. Moshawan, Y. Wang, X. Qu, Z.-G. Chen, J. Zou, Chem. Sci. https://doi.org/10.1039/C8SC02397B (2018)
35. P.J. Price, Philos. Mag. **46**, 1252 (1955)